The 4th INTERNATIONAL WORKSHOP ON FUNDAMENTAL ISSUES,
APPLICATIONS AND FUTURE RESEARCH DIRECTIONS FOR
PARALLEL MECHANISMS / MANIPULATORS / MACHINES,
BELFAST, UK, 25-26 JUNE 2020

Coupler Pose Curves for Planar 4R Mechanisms

Zachary A. COPELAND [a,1], M. John D. HAYES [b]
[a] *PhD Student, Carleton University, Department of Mechanical and Aerospace Engineering*
[b] *Professor, Carleton University, Department of Mechanical and Aerospace Engineering*

Abstract. This paper will begin to lay the foundation to solving the continuous approximate Burmester problem using a technique to map desired continuous coupler pose curves to the closest, in some sense, quartic curve of intersection of two quadric dyad constraint surfaces in the planar kinematic mapping image space. Since there are 27 distinct planar 4R mechanism types with specific input-output mobility constraints, the first step in the path forward is to examine the corresponding image space quartic curves corresponding to the coupler pose curves of these linkage types. This paper provides first steps towards characterisation of the family of quartic coupler pose curves generated by several examples among the 27 planar 4R linkage types.

Keywords. Planar kinematic mapping image space, continuous approximate Burmester problem, first-species space-quartic.

1. Introduction

The study of planar four bar linkages involves a large variety of problems ranging from the problem of guiding a point along a specific curve (the *coupler curve*) to the input-output relationship of the crank and follower (the *function generation* problem), to rigid body guidance of the coupler (the *Burmester* problem), to trajectory generation and the transmission of forces and torques through the linkage; in this paper, the topic will be restricted to the Burmester problem. In most cases, the Burmester problem involves guiding a rigid body through a discrete sequence of positions and corresponding orientations (poses), and identifying the linkage that best guides this rigid body through the discrete number of poses, with no real control over the intermediate configurations.

Burmester theory [1] states that five finitely separated rigid body poses are sufficient to identify at most four dyads that can be taken two at a time: there can be as many as

[1] Corresponding Author: Zachary A. Copeland, PhD Student, Carleton University, Dept. of Mech. and Aero. Engineering, 1125 Colonel By Dr., Ottawa, Canada; E-mail: zack.copeland@carleton.ca

six different four-bar mechanisms that can guide a rigid body exactly through five specified poses. The discrete approximate Burmester problem specifies greater than five poses leading to an optimisation problem to identify a linkage that best approximates the specified poses in some sense. Whereas, the continuous approximate Burmester problem, an extension of the continuous approximate synthesis problem for function-generation [2], considers a continuous pose curve to which the best approximating linkage must be fit, in some sense.

Solutions to any form of the Burmester problem include branch-defect and assembly mode issues [3], as well as ordering of the desired poses. The identified linkage will be able to guide the coupler through the desired poses, though whether or not the coupler will be able to reach all poses in the same assembly mode, or the order in which these poses will be assumed is not guaranteed. While there are algorithms and extended solution characterisations which determine whether or not an assembly mode defect or an ordering fault is present within the synthesised linkage exist, these algorithms are inherently retrospective and are performed as an analysis on the synthesised linkage. Ideally, a full solution to the Burmester problem would be able to present all of this information, and remove the need for any further analysis.

In this paper, we intend to layout the goal of taking a desired continuous parametric pose curve of arbitrary complexity described in the Euclidean plane and identifying the planar 4R linkage that best approximates the desired motion, in some specified sense, over the continuous range of motion. This is certainly *work in progress* and we will offer no results per se, rather the intended path towards attaining the goal.

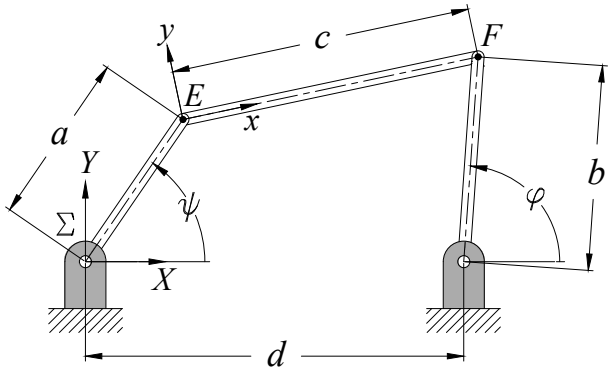

Figure 1. A planar 4R mechanism.

2. Kinematic Mappping Image Space

A general displacement of one coordinate system in the plane relative to a stationary one requires three independent parameters to fully describe it. With reference to Figure 1, the position of a point in the moving coordinate system E, described by the ratios $(x : y : z)$, can be mapped to the coordinates of the same point, but described by the ratios $(X : Y : Z)$, in the stationary coordinate system Σ using a homogeneous linear transformation as:

$$\begin{bmatrix} X \\ Y \\ Z \end{bmatrix} = \begin{bmatrix} \cos\varphi & -\sin\varphi & a \\ \sin\varphi & \cos\varphi & b \\ 0 & 0 & 1 \end{bmatrix} \begin{bmatrix} x \\ y \\ z \end{bmatrix} = \begin{bmatrix} -X_3^2+X_4^2 & -2X_3X_4 & 2X_1X_3+2X_2X_4 \\ 2X_3X_4 & -X_3^2+X_4^2 & -2X_1X_4+2X_2X_3 \\ 0 & 0 & X_3^2+X_4^2 \end{bmatrix} \begin{bmatrix} x \\ y \\ z \end{bmatrix}. \quad (1)$$

The Cartesian coordinates of the origin of E measured in Σ are (a,b), while φ is the rotation angle measured from the X-axis to the x-axis, the positive sense being counter-clockwise. Clearly, in the first matrix in Eq. (1) the three characteristic displacement parameters are (a,b,φ). Image points in the 3-D projective image space are defined in terms of the displacement parameters (a,b,φ) as [5]

$$(X_1 : X_2 : X_3 : X_4) = ((a\sin(\varphi/2) - b\cos(\varphi/2) : (a\cos(\varphi/2) + b\sin(\varphi/2) : 2\sin(\varphi/2) : 2\cos(\varphi/2)). \quad (2)$$

The second matrix in Eq. (1) is the Euclidean displacement transformation from the first matrix expressed in terms of the image space coordinates as defined in Eq. (2). In order for a set of four numbers, a point in the image space, to represent a planar displacement it must be that $X_3^2 + X_4^2 \neq 0$, given the definitions of X_3 and X_4. Considering rotations of π as special cases, we can safely project the image space coordinates into the hyperplane $X_4 = 1$ leaving

$$(X_1 : X_2 : X_3) = \left(\frac{1}{2}(a\tan(\varphi/2) - b) : \frac{1}{2}(a + b\tan(\varphi/2)) : \tan(\varphi/2)\right). \quad (3)$$

Extracting the pose from the full or the normalised image space coordinates is given by:

$$\varphi = 2\tan^{-1}(X_3/X_4); \quad a = \frac{2(X_1X_3 + X_2X_4)}{(X_3^2+X_4^2)}; \quad b = \frac{2(X_2X_3 - X_1X_4)}{(X_3^2+X_4^2)}. \quad (4)$$

2.1. Image Space Constraint Surface

In the projective extension P^3 of the Euclidean plane E^2 an RR-dyad can be modelled as the motion of a fixed point in E constrained to move on a fixed centred circle with constant radius in Σ, where the circle can be describe as

$$k_0(X^2+Y^2) + k_1XZ + k_2YZ + k_3Z^2 \;=\; 0. \quad (5)$$

The k_i represent the quadric shape parameters. When $k_0 = 1$ Eq. (5) describes a circle and the parameters are defined as

$$k_0 = 1, \;\; k_1 = -X_c, \;\; k_2 = -Y_c, \;\; k_3 = k_1^2 + k_2^2 - r^2. \quad (6)$$

Here X_c, Y_c represent the Cartesian (X,Y) coordinates of the circle centre in Σ while r is it's radius. Upon substitution of Eq. 1 into Eq. 5 the following quadric in the X_i is revealed, after factoring out the term $1/4(X_3^2+X_4^2)$, which can never vanish:

$$k_0 z^2(X_1^2+X_2^2)+\frac{1}{4}\left[k_0(x^2+y^2)+k_3z^2-2z(k_1x+k_2y)\right]X_3^2+$$
$$\frac{1}{4}\left[k_0(x^2+y^2)+k_3z^2+2z(k_1x+k_2y)\right]X_4^2+(k_1z^2-k_0xz)X_1X_3-(k_2z^2+k_0yz)X_1X_4+$$
$$(k_2z^2-k_0yz)X_2X_3+(k_0xz+k_1z^2)X_2X_4+(k_2xz-k_1yz)X_3X_4 \;=\; 0. \quad (7)$$

When we remove the one parameter family of image points for orientations of π we can, for convenience, normalise the image space coordinates and use the definitions for the X_i from Eq (3) making $X_4 = 1$. Since we are only interested in real finite linkages we can also set $Z = z = 1$. What remains is a hyperboloid of one sheet, projected into the hyperplane $X_4 = 1$, which has circular sections in every plane parallel to $X_3 = 0$ [8]:

$$k_0(X_1^2+X_2^2)+\frac{1}{4}\left[k_0(x^2+y^2)+k_3-2(k_1x+k_2y)\right]X_3^2+$$
$$(k_1-k_0x)X_1X_3+(k_2-k_0y)X_2X_3-(k_2+k_0y)X_1+(k_0x+k_1)X_2+$$
$$(k_2x-k_1y)X_3+\frac{1}{4}\left[k_0(x^2+y^2)+k_3z^2+2z(k_1x+k_2y)\right] \;=\; 0. \quad (8)$$

The point (x,y) is represented by the Cartesian coordinates of a specified point on the coupler link described in moving frame E, see Figure 1. The motion of the coupler can be visualised as the intersection curve of two hyperboloids of one sheet which define the motion constraints of left and right dyads of a given 4R linkage. The X_1 and X_2 coordinates contain the (a,b) coordinates of the origin of E for any given φ parameter on the X_3-axis. Hence, the 4^{th} order curve of intersection of the two quadric constraint surfaces completely describes the coupler motion, since every point on the continuous curve describes the different (a,b,φ) parameters of the coupler for given values of the 4R input link angle.

The intersection of two second order surfaces will always generate a fourth order curve; these curves can self-intersect, lie in separate branches, and may have complex-conjugate components. Fourth order curves can always be classified into two classes of function; quartics of the first species are the intersection, or base, of a pencil of quadric surfaces, while quartics of the second species lie only on one quadric surface [6]. Given the formulation at hand, specifically that the coupler pose curves are generated through the intersection of at least two and at most four quadric surfaces, it is clear that these surfaces are, by definition, quartics of the first species. General quartic surfaces can be defined by nine distinct points [6], however, Burmester showed [1] that only five distinct poses (five points in the kinematic mapping image space) are required to uniquely define the pencil of at most four quartics which define dyads that, when combined into a 4R linkage, can make the coupler coordinate system exactly visit the five specified poses. Hence, the image space constraint hyperboloids of one sheet are not general quadrics. The special nature of the constraint surfaces represent four constraints common to all quadric constraint hyperboloids.

The hyperboloids, corresponding to RR-dyads, always intersect planes parallel to $X_3 = 0$ in circles. Thus, all constraint hyperboloids contain the image space equivalent of the *imaginary circular points*, J_1 and J_2: $(1 : \pm i : 0 : 0)$ [5]. The points J_1 and J_2 are imaginary points on the real line l of intersection of the planes $X_3 = 0$ and $X_4 = 0$. This

real line is the axis of a pencil of planes that includes the complex conjugate planes V_1 and V_2, defined by: $X_3 = \pm iX_4$. The hyperboloids all have V_1 and V_2 as tangent planes, though not necessarily at J_1 and J_2. Since all RR-dyad hyperboloids share these four constraints in their shape parameters, only five additional constraints need be imposed: the five desired poses.

2.2. 4R Linkage Architecture

Mobility constraints on the input and output links for planar 4R mechanisms are linked to specific conditions on link lengths a, b, c, and d as illustrated in Figure 1. These conditions, developed in [9] and later refined in [7], depend on the value of three sums of link lengths being either greater than, identically equal to, or less than zero. The three sums are (maintaining the naming convention from [7] to maintain consistency):

$$\begin{aligned} A_1: &\quad a-b-c+d; \\ C_1: &\quad a+b-c-d; \\ D_1: &\quad a-b+c-d. \end{aligned} \tag{9}$$

The three permutations of $+$, $=$, and $-$ for each of the sums A_1, C_1, and D_1 lead to 27 unique combinations that represent all planar 4R linkage input-output mobility types[2], listed in Table 1 [7].

Table 1. Planar 4R types classified by mobility conditions.

Type	A_1	C_1	D_1	Input	Output	Type	A_1	C_1	D_1	Input	Output
1	+	+	+	0-rocker	0-rocker	15	0	0	-	crank	π-rocker
2	+	+	0	0-rocker	0-rocker	16	0	-	+	π-rocker	crank
3	+	+	-	rocker	rocker	17	0	-	0	crank	crank
4	+	0	+	0-rocker	crank	18	0	-	-	crank	π-rocker
5	+	0	0	0-rocker	crank	19	-	+	+	crank	crank
6	+	0	-	0-rocker	π-rocker	20	-	+	0	crank	crank
7	+	-	+	rocker	crank	21	-	+	-	π-rocker	π-rocker
8	+	-	0	0-rocker	crank	22	-	0	+	crank	crank
9	+	-	-	0-rocker	π-rocker	23	-	0	0	crank	crank
10	0	+	+	crank	crank	24	-	0	-	crank	π-rocker
11	0	+	0	crank	crank	25	-	-	+	π-rocker	0-rocker
12	0	+	-	π-rocker	π-rocker	26	-	-	0	crank	0-rocker
13	0	0	+	crank	crank	27	-	-	-	crank	0-rocker
14	0	0	0	crank	crank						

Perhaps the most important step in developing a continuous Burmester synthesis algorithm is understanding the algebraic nature of the possible coupler pose curves implied by the 4R linkage types listed in Table 1. Since the major goal of this paper is to derive parametric equations of the 4^{th} order curve of intersection of the associated quadric constraint surfaces, several linkages are identified that each fit one of the mobility types listed in the table.

[2]When the X-axis of the stationary coordinate system Σ, whose origin is located at the centre of the left-most ground fixed joint points towards the centre of the other ground fixed joint, as in Figure 1, then for the link connected to the joint: a *rocker* rocks in the range between 0 and π radians; a 0-rocker rocks in the range between $-\pi/2$ and $\pi/2$; and a π-rocker rocks in the range between $\pi/2$ and $3\pi/2$.

2.2.1. Linkage Type 2: 0-rocker-0-rocker

The link lengths for the linkage were selected as $(a,b,c,d) = (3,2,1,2)$. For the input-dyad (the left-most dyad) the circle parameters are $(k_0,k_1,k_2,k_3) = (1,0,0,-9)$ and for the output-dyad are $(k_0,k_1,k_2,k_3) = (1,-2,0,0)$. The corresponding two constraint surfaces and curve of intersection are illustrated in Figure 2. As is seen in Figure 2b, the

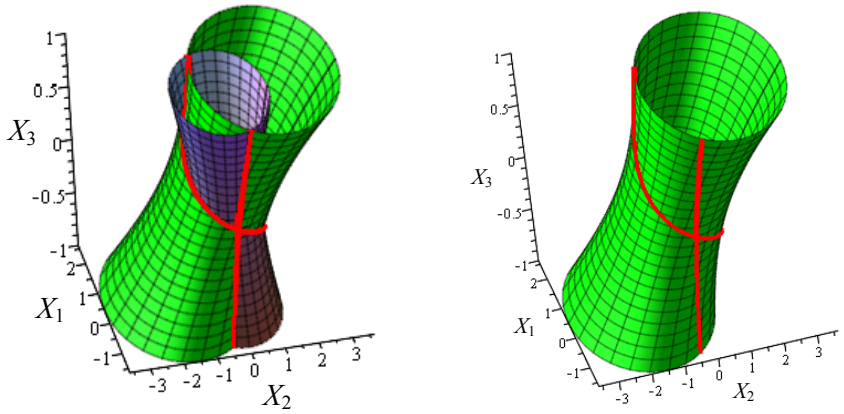

(a) Both hyperboloids and intersection.

(b) One hyperboloid and intersection.

Figure 2. Type 2 constraint hyperboloids and curve of intersection.

coupler pose curve in the image space has a single self-intersection, confirming results in [3]. But, what is new, combined with the input-output mobility in Table 1, is that for this 0-rocker-0-rocker the coupler has a branch point, where at a particular position and orientation, it can take one of two paths on the coupler curve. Moreover, because the intersection curve goes to infinity in two directions along the X_3-axis, the coupler can rotate completely through 2π radians.

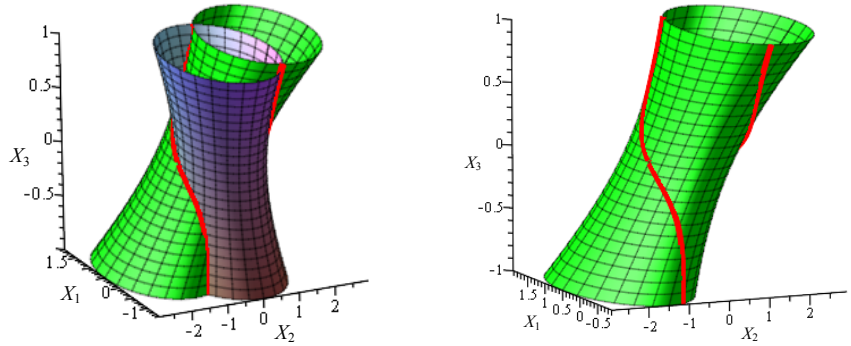

(a) Both hyperboloids and intersection.

(b) One hyperboloid and intersection.

Figure 3. Type 3 constraint hyperboloids and curve of intersection.

2.2.2. Linkage Type 3: rocker-rocker

The link lengths for the Type 3 linkage were selected as $(a,b,c,d) = (2,2,1,2)$. For the input-dyad (the left-most dyad) the circle parameters are $(k_0,k_1,k_2,k_3) = (1,0,0,-4)$ and for the output-dyad are $(k_0,k_1,k_2,k_3) = (1,-2,0,0)$. The corresponding two constraint surfaces and curve of intersection are illustrated in Figure 3. As can be seen in the figure, what is different for this Type 3 rocker-rocker compared to the Type 2 0-rocker-0-rocker is that the coupler pose curve in the image space possesses no finite self-intersections and hence there are no branch points. Since the curve of intersection extends to infinity in both directions along the X_3-axis the coupler can rotate completely through 2π radians.

2.2.3. Linkage Type 9: 0-rocker-π-rocker

The link lengths for this Type 9 linkage, a 0-rocker-π-rocker are $(a,b,c,d) = (1,2,1,3)$. For the input-dyad (the left-most dyad) the circle parameters are $(k_0,k_1,k_2,k_3) = (1,0,0,-1)$ and for the output-dyad are $(k_0,k_1,k_2,k_3) = (1,-3,0,5)$. The corresponding two constraint surfaces and curve of intersection are illustrated in Figure 4. The coupler pose curve is affinely finite, and agrees with the results from [3].

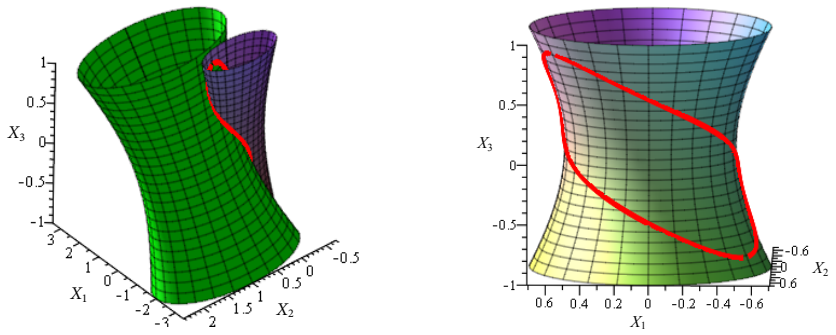

(a) Both hyperboloids and intersection.

(b) One hyperboloid and intersection.

Figure 4. Type 9 constraint hyperboloids and curve of intersection.

2.2.4. Linkage Type 27: crank-0-rocker

The final linkage considered is a crank-0-rocker of Type 27. The linkage was identified from a set of five poses listed in [3] that should correspond to a linkage that generates two distinct affinely finite pose curves in the kinematic mapping image space. The resulting link lengths identify it as a Type 27 linkage.

The five poses were used to identify constraint hyperboloids, following the method in [10]. In agreement with Burmester theory, four RR-dyad constraint surfaces were identified, see Figure 5. Each pair of constraint surfaces intersects in a distinct pair of closed curves of intersection. However, all eight of the corresponding curves intersect in the same five points, the poses specified at the outset. The initial expectation was that the four quadrics would lay in a pencil on a single curve of intersection, however this is not the case.

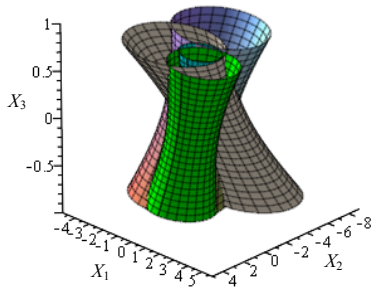

Figure 5. Four hyperboloids.

3. Conclusions

The conclusion we wish to draw from the work presented herein is that it may be possible to develop a kinematic mapping based algorithm to solve the continuous approximate Burmester problem. It is to be seen that the constraint hyperboloids corresponding to pairs of RR-dyads intersect in 4^{th} order curves. It is expected that a study of the algebraic properties of these spatial quartic curves will lead to a method to identify the planar 4R linkage that best approximates, in some least-squares sense, a desired parametric coupler pose curve. This will yield an interesting lower bound on solutions to the discrete approximate Burmester problem.

References

[1] L. Burmester, *Lehrbuch der Kinematik*. Arthur Felix Verlag, Leipzig, Germany, 1888.

[2] A. Guigue and M.J.D. Hayes, *Continuous Approximate Synthesis of Planar Function-generators Minimising the Design Error*. Mechanism and Machine Theory, 101 (2016): 158-167.

[3] H.P. Schrocker, M.L. Husty, J.M. McCarthy, *Kinematic Mapping Based Assembly Mode Evaluation of Planar Four-Bar Mechanisms*. ASME Journal of Mechanical Design, 129(9) (2007) 924-929.

[4] B. Ravani and B. Roth, *Motion Synthesis Using Kinematic Mappings*. ASME, J. of Mechanisms, Transmissions, & Automation in Design, 105 (1983) 460-477.

[5] O. Bottema and B. Roth, *Theoretical Kinematics*. Dover Publications, Inc., New York, N.Y., U.S.A., 1990.

[6] D.M.Y Sommerville, *Analytical Geometry of Three Dimensions*. Cambridge University Press, England, 1934.

[7] M.J.D. Hayes, M. Rotzoll, and M.L. Husty, *Design Parameter Space of Planar Four-bar Linkages*. Proceedings of the 15th IFToMM World Congress, Krakow, Poland, 229-238, 2019.

[8] M.J.D. Hayes and M.L. Husty, *On the Kinematic Constraint Surfaces of General Three-legged Planar Robot Platforms*. Mechahnism and Machine Theory 38(5) (2003) 379-394.

[9] A.P. Murray and P.M. Larochelle, *A Classification Scheme for Planar 4R, Spherical 4R, and Spatial RCCR Linkages to Facilitate Computer Animation*. Proceedings of the 1998 ASME Design Engineering Technical Conferences (DETC'98), Atlanta, Georgia, U.S.A., 1998.

[10] M.J.D. Hayes and P.J. Zsombor-Murray, *Solving the Burmester Problem Using Kinematic Mapping*. Proceedings of the ASME Design Engineering Technical Conferences: Mechanisms Conference, Montréal, QC, Canada, on CD, 2002.